Simulation Studies of the Directivity in Detection of Solar Neutrinos Using Deep Sea Water*

Yan Zhou,[1,†] Dawei Si,[1] Sheng Xiao,[1] Junhuai Xu,[1] Xin Chen,[1] and Zhigang Xiao[1,‡]

[1]*Department of Physics, Tsinghua University, Beijing 100084, China*

Čerenkov detector has its advantage to construct the reaction vertex and incident direction of the energetic particles, and thus to locate the emission source. We propose to measure the neutrino source by modular photomultiplier tube (PMT) array using clean and transparent deep sea water as sensitive medium. The feasibility of the detection of solar neutrino is demonstrated by full simulation based on Geant4 packages. The production and transport of Čerenkov photons generated by the ν_e-e^- scattering are simulated. Houth transform method is applied to reconstruct the vertex and the direction of the high-speed electron, as well as the incident direction of the neutrinos. The dominant background of γ radiation from ^{40}K in sea water can be suppressed by a factor of 10^7 if a threshold on the number of firing PMTs is introduced. The total reconstruction efficiency increases with the incident energy, reaching 25% for 6 MeV neutrino and 52% for 10 MeV neutrino, respectively. To locate an existing neutrino source, a certain number of neutrino events are required, depending on the background intensity above the threshold. The simulation results reveal how feasible to measure solar neutrino ν_e using deep sea water.

Keywords: neutrino, Čerenkov , Geant4, Energy Resolution, Direction Reconstruction, Hough Transform

I. INTRODUCTION

Neutrinos with energies of a few MeV or higher are one kind of the major products in nuclear reactions, both in the Sun (electron-neutrino ν_e) or in the terrestrial nuclear reactors (anti-electron neutrino $\bar{\nu}_e$). Detection of these neutrinos from the sun provides a test of the standard solar model (SSM), leading to the discovery of the neutrino oscillation [1, 2], while the detection of the anti electron-neutrinos helps to monitor the operational status of nuclear reactors [3–9], as well as to constrain the oscillation angle θ_{13} between the first and the third generation neutrinos [10, 11]. From a practical point of view, however, the detection of neutrinos is extremely difficult because they are involved only in weak interactions with small cross sections. Despite these extreme difficulties, many types of neutrino detectors have been invented since the first direct detection of neutrino event [12–15]. While the inverse beta decay (IBD) method has been widely used to detect the anti electron neutrino ($\bar{\nu}_e$), the detection of the electron neutrino (ν_e) can be achieved by making use of the elastic scattering of ν_e with electrons. The advantage of the ν_e-e^- elastic scattering is that the direction of the recoil electron is closely aligned with the direction of the incident neutrino, depending on the ν_e energy [24].

Water Čerenkov detector is a widely used neutrino detector. For instance, the Super-Kamiokande detector (Super-K) utilizes roughly 40 kT of pure water to detect the solar neutrinos, supernova neutrinos, and cosmic ray neutrinos with great success [25]. When the recoil electron gains kinetic energy and moves with a velocity greater than the speed of light in water, Čerenkov radiation are emitted at a certain angle and transmitted to the photo-multiplier tubes (PMTs), which respond sensitively with high timing resolution. As long as the vertex and the trajectory of the recoil electron are reconstructed, the direction of the incident neutrino can be inferred.

To further improve the detection ability in terms of event rate, increasing the volume of the detector becomes less effective in land-based laboratories due to the rapidly increasing technical challenges. To achieve a mega volume of detection material to catch the ν_e-e^-scattering event, it has been proposed to use clean water under the sea or ice at the South Pole of the earth as the target material, see [16, 17] for example. This approach has indeed been realized to detect extremely high-energy neutrinos at various experiments [18–23]. Moving to low energy domain, however, is still challenging because of the intense background produced by natural radiation sources like ^{40}K and ^{208}Tl, as well as other radioactive isotopes produced in cosmic ray induced reactions. Before reaching a convincing conclusion in this direction, enormous simulations studies are certainly required.

In this paper, we explore the feasibility of detecting the solar neutrinos using seawater as the target material based on Monte Carlo simulations. We focus on the reconstruction of the incident direction of the neutrinos with the faint Čerenkov light signals, as well as on the suppression of the intense radiation background. The paper is organized as follows. Section II introduces the software, the detection array construction, and the optical process modeling. Section III presents the method of the event reconstruction. Section IV describes the influence and suppression of the background. Section V provides the summary.

II. SIMULATION SOFTWARE

The simulations are conducted within the framework of WCSim [26], which is a full analysis framework developed by the Super-K collaboration based on Geant4 packages. It includes the detector construction, transport of products from neutrino-induced reactions in water, the generation and propagation of the Čerenkov lights and the response of the PMTs.

* Supported by the Ministry of Science and Technology under Grant Nos. 2023YFC3107401 and by Tsinghua University Initiative Scientific Research Program.

† zhou-y21@mails.tsinghua.edu.cn

‡ xiaozg@tsinghua.edu.cn

In this section, we present the simulation procedures.

A. Detector constructions

In the current application, water is defined as the absorption material, and the PMTs distributed in a certain configuration, absorb the Čerenkov light emitted by the high-speed electrons produced in the neutrino-induced reactions. For simplicity in this startup simulation, we adopt a spherical distribution of the PMTs in water. The radius of the sphere, at the front surface of the PMTs, is set to $R = 5\mathrm{m}$, which is reasonable and feasible to build as a demonstrator. To achieve a uniform distribution on a sphere, the positions of the PMTs are placed according to the Fibonacci grid [27].

$$\begin{cases} \cos\theta_i = \frac{2i+1}{N} - 1 \\ \phi_i = (\sqrt{5}-1)i\pi \end{cases} \quad (i \in [1, N]) \tag{1}$$

The symmetrical axis of each PMT is aligned with the center of the sphere. The diameter of the sensitive area of each PMT is $\phi_{\mathrm{pmt}} = 8$ inches. To cover 30% of the entire sphere surface, a total of 2906 PMTs are constructed. The physical construction of the PMT is simplified as a glass bulb containing vacuum inside. The remaining area of the sphere is covered by black sheets to reduce reflection inside the sphere, i.e., the reflectivity of the sphere's surface is set to 95% from the inner to outer space. In order to circumvent the residual radiation from the materials of the PMTs, the fiducial volume is defined by the sphere with a radius of $R_{\mathrm{fd}} = 4.5$ m. Fig. 1 presents the schematic view of the PMT sphere. The distance between neighboring PMTs is 30-40 cm.

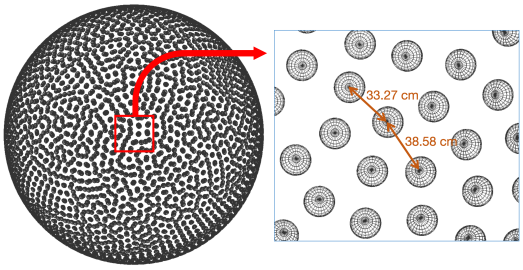

Fig. 1. (Color online) The schematic view of the PMTs distributing on a sphere filled by water.

B. Simulation of the Optical process by incident electron

The simulated event begins with the generation of a charged particle in the neutrino induced reaction, which is turned on compulsorily because the cross section of weak interactions is too low to ensure sufficient statistics with conventional sampling techniques. The charged particle loses energy in water and emits Čerenkov light if the speed is above the threshold. The simulation process follows every secondary particles until being stopped or absorbed. The Čerenkov photons in water experience scattering and absorption according to the optical parameters. If the photon finally arrives at the surface of the PMT, a certain number of photon electrons (PEs) can be produced to deliver a signal according to the response parameter settings of the PMTs. Alternatively the photons may also be absorbed if they hit on the black surface out of the acceptance of the PMT surface. Here our PMT response setting is the same with that of Super-K experiment[28]. If more than 10 PMTs are fired within 50 ns, the trigger signal will be generated and the data are stored on disk for further analysis.

Therefore, the transport and absorption of the Čerenkov photons is the key process of the detection. The process is defined by a few optical parameters for the medium and the surfaces, including the absorption length, refraction index and scattering length. All the parameters are dependent on the wave length of the photons. For the water, we simply adopts the parameter set of Super-K [28], which is applicable for pure water but not necessarily suitable for sea water. Nevertheless, for the current stage of the simulation, the selection of the parameters will not bring significant influence to the conclusion. The average absorption length is 100 m, refraction index is 1.334, and the scattering lengths is 200 m. In addition, the refraction index for glass is set to 1.6, and the absorption length for black sheet is 10^{-11} m. All surfaces we defined are just the surface between these mediums. The reflectivity between water and black sheet is set to 0.05. The quantum efficiency of PMT is set to be a function of photon wavelength, as shown in Fig. 2. The maximum value is 21.1% at $\lambda = 400$ nm.

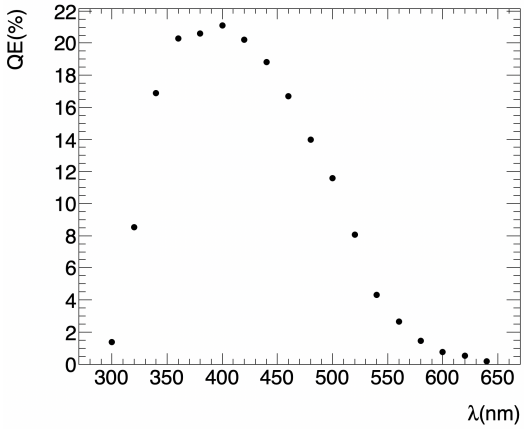

Fig. 2. PMT quantum efficiency as a function of photon wavelength. Data is taken from [26].

Figure 3 presents an event display of the optical process as a result of the reaction induced by a 6 MeV electron neutrino. The incident direction is set randomly in 4π solid angle and the vertex is fixed at the center. The red lines represent the tracks of the Čerenkov photons, while the dashed arrow denotes the direction of the recoil electron, which one expects to construct from the PMTs fired by the photons, while the rest photons absorbed by the water or the sphere surface will be lost and excluded in the analysis.

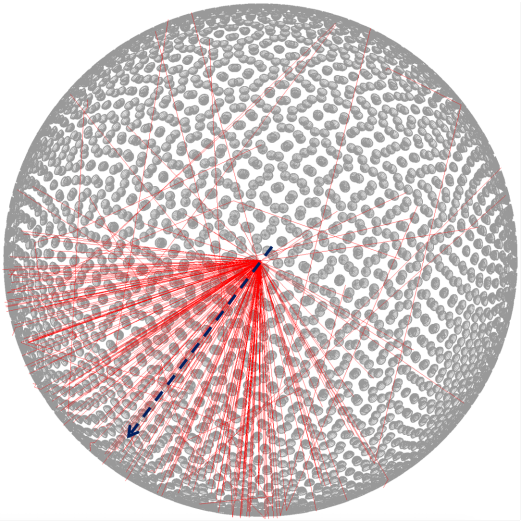

Fig. 3. (Color online) One event display induced by a 6 MeV electron neutrino. The red lines are the tracks of the Čerenkov photons and the thick dashed black arrow denotes the recoil electron in ν_e-e^- scattering.

Figure 4 presents the scattering plot of the photons firing the PMTs vs the total number of the photons produced in each neutrino induced reactions. Dark noise of 4.2 kHz is considered in the simulation. It is shown that the overall efficiency of firing the PMT is about 20%. Considering the geometric coverage is about 30%, one can infer that about 40% photons are lost in the transport to the PMT by scattering or absorption.

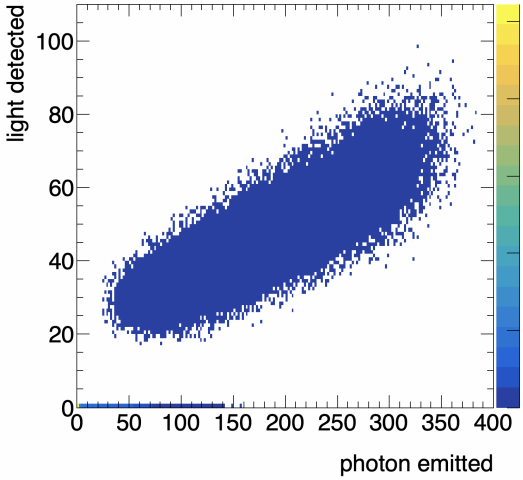

Fig. 4. (Color online) The correlation of the number of the emitted Čerenkov photons and the detected ones.

The distribution of the Čerenkov photons with limited number is crucial for event reconstruction at event-by-event basis. Figure 5 presents the distribution of the Čerenkov photons in the polar coordinate system of θ $vs.$ ϕ. Here the θ is the angle between the direction of the recoil electron and the vector from the vertex of the reaction to the fired PMTs, and ϕ is the azimuthal angle of the Čerenkov photon. Panel (a) displays the accumulative plot of θ $vs.$ ϕ for 10^5 events with the incident direction of the electron pointing to the pole ($\theta = 0°$) by definition. It is shown that the Čerenkov circle is evidently presented with the center at $\theta = 0°$. For a single event, however, as in panel (b) and (c) for examples, the fired PMTs distribute in a rather scattered manner, exhibiting an invisible circular pattern by eye. And hence, it requires a sophisticated algorithm to reconstruct the direction of incident electron.

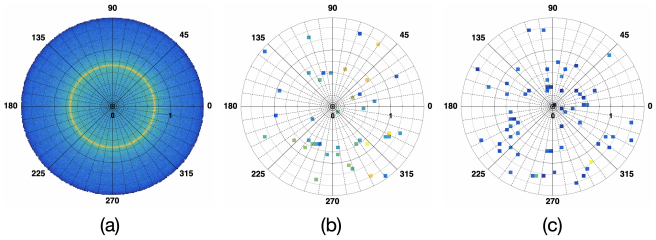

Fig. 5. (Color online) Projection diagram of fired PMTs relative to the recoil electron direction. (a) Integration over 10^5 events. (b) and (c), Fired PMT distributions in two single events.

III. EVENT RECONSTRUCTION

Next, we present the reconstruction procedure for the ν_e-e^-scattering event. The task of the reconstruction is to find the timing and vertex of the scattering from the detected Čerenkov photons.

A. Vertex reconstruction

We consider only the ν_e-e^-elastic scattering process. The determination of the vertex position relies on the timing information of the fired PMTs. Thus the time resolution is an essential performance parameter. For the neutrinos with a few MeV kinetic energy, the recoil electron loses all kinetic energy rapidly, thus the track length of the electron is ignored and all the Čerenkov photons are originated from a single point by assumption, written as (x_0, y_0, z_0, t_0). Given the exact position $(x_\mathrm{i}, y_\mathrm{i}, z_\mathrm{i})$ of each fired PMT, one can expect the timing that the Čerenkov photon travels to the i^{th} fired PMT $t_\mathrm{i}^{\mathrm{exp}}$ as

$$t_\mathrm{i}^{\mathrm{exp}} = t_0 + \frac{\sqrt{(x_\mathrm{i}-x_0)^2+(y_\mathrm{i}-y_0)^2+(z_\mathrm{i}-z_0)^2}}{c/n} \quad (2)$$

Comparing the real firing time recorded by the PMT and the expected time from eq.(2) for all fired PMTs, we could choose the parameters for the vertex that makes them consistent the most as the final constructed vertex.

Our specific way to achieve this idea is to minimize the function in eq.(3)[29]

$$f = \sum \exp\left(-\zeta_\mathrm{i}^2/\sigma_\mathrm{t}^2\right) \quad (3)$$

where $\zeta_{\rm i} = t_{\rm i} - t_{\rm i}^{\rm exp}$ is the deviation of measured time $t_{\rm i}$ from the expected value $t_{\rm i}^{\rm exp}$, and $\sigma_{\rm t}^2 = 50$ represents the PMT time resolution. It is shown that the ansatz (3) without taking the exponential operation is like a conventional χ^2 value. The reason to add the exponential term is that some Čerenkov lights can be reflected many times before hitting a certain PMT, which makes the real firing time far away from the calculated one by Eq. (2). The exponential term can make the fit less sensitive to those points and achieve a more reasonable reconstruction of the vertex based on the event-by-event logics.

B. Direction construction

The Čerenkov lights generally form a cone with semi-apex angle satisfying $\sin\alpha = (n\beta)^{-1}$. Since the electron with energy of several MeV travels a short distance (about 1 cm) before slowing down to the threshold, one assumes the Čerenkov lights are emitted from the reaction vertex with the emission angle $\alpha_{\rm c} \approx \arcsin(n^{-1})$. Considering the secondary scattering of the electrons in the medium, the final angular distribution exhibits a broadening, as shown in Fig. 6. The distribution will be adopted as the possibility distribution function (PDF) in Hough transform, see next.

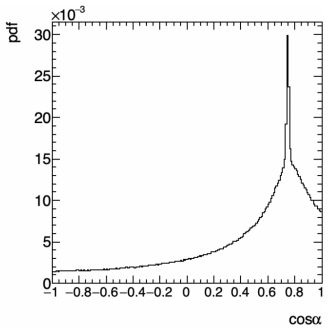

Fig. 6. Angular distribution of Čerenkov lights with respect to the electron flying direction.

The Hough transform (HT) method [30] is applied to extract the direction of recoil electron of the ν_e-e^- scattering from the information recorded by the PMTs. To elucidate the HT method, Fig. 7 presents the procedure taking the event example shown in the Fig. 5 (b). After getting a constructed vertex, each fired PMT i defines a direction vector described by the polar angle $\theta_{\rm i}$ and the azimuth $\phi_{\rm i}$. By assuming a fixed Čerenkov angle $\alpha_{\rm c}$ for simplicity, the data point of each PMT would generate a circle on the θ-ϕ plane at the given polar angle $\alpha_{\rm c}$ with respect to the longitudinal axis being from the vertex to the fired PMT, as shown in the panel (a) by the red cross symbols for examples. This circle transforms a probability distribution in the parameter space of the electron direction characterized by θ_0 and ϕ_0. Next, As shown in panel (b), summing up the transformed probability distributions weighted by PE number from all fired PMT data points, one obtains the probability distribution of finding the high speed electron in θ-ϕ plane, and the most probable point can be regarded as the constructed direction for the electron. In real calculations, because of the scattering of the Čerenkov photons, one shall use the PDF of the Čerenkov angle in Fig. 6 instead of a fixed value $\alpha_{\rm c}$. Then following the same procedure, one arrives at the real probability distribution of the direction in θ-ϕ parameter space, and obtains the most probable point θ_0-ϕ_0, as depicted by the read cross marker in Fig. 7 (c).

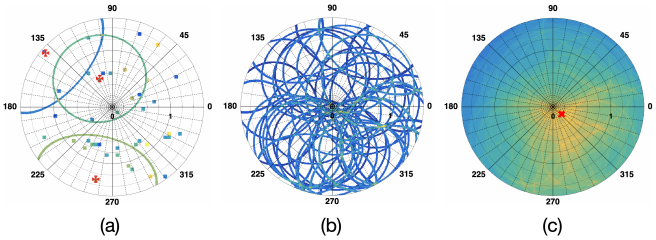

Fig. 7. (Color online) Schematic elucidation of the Hough Transform method. (a) The fired PMTs on θ-ϕ plane, the circles near the red cross markers are the possibility distribution to find the electrons, assuming a constant Čerenkov angle. (b) All the possibility distributions are summed up for all fired PMTs with the number of PE as the weight. (c) The real possibility distribution of finding the electron in θ-ϕ parameter space, using the PDF shown in Fig. 6. The red cross marker represents the recognized direction of the electron.

C. Result from neutrino events

In the simulations of neutrino-induced reactions, in order to solve the problem that the cross-section is too small to have sufficient statistics, we force the reaction to occur when injecting a neutrino, and the distribution of the recoil electrons are sampled using eq.(4)[31] shown below

$$\frac{d\sigma}{d\cos\theta} = \frac{4\sigma_0 E_\nu^2 M^2 \cos\theta}{(M^2 - E_\nu^2\cos^2\theta)^2}\left(g_1^2 + g_2^2 - W_{\rm g}\right) \quad (4)$$

The term $W_{\rm g}$ reads

$$W_{\rm g} = \frac{2g_2 m_e \cos^2\theta\,(g_2 E_\nu + g_1 m_e)}{M^2 - E_\nu^2\cos^2\theta} \quad (5)$$

where g_1, g_2 are two constants relevant to the flavour of neutrinos, $M = m_e + E_\nu$. For the solar neutrinos $\nu_{\rm e}$, the corresponding distribution is shown in Fig. 8. The reaction vertex is randomly distributed in the fiducial volume of the detector setup. Once the recoil electron is sampled, Čerenkov lights are generated according to the velocity of the recoil electron before being transported to the PMTs, where the emitted PEs are recorded. Then one can apply the HT method to reconstruct incident direction of the recoil electron and the position of the reaction vertex.

Fig. 9 presents the results of the reconstruction. For each energy point, 10^5 events are simulated. Panel (a) presents

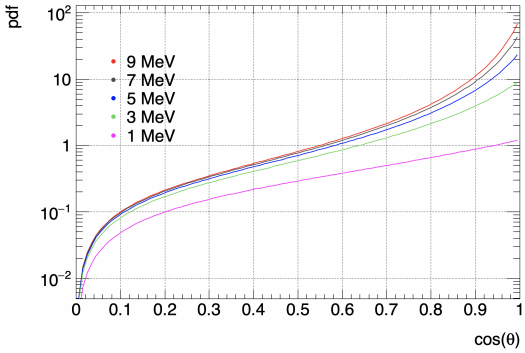

Fig. 8. (Color online) Angular distribution of the recoil electron in $\nu_e e^-$ scattering with respect to the incident direction of the neutrino at different E_ν.

the distribution of α, defined as the angle between the reconstructed direction and the genuine direction of the recoil electron. It is shown that, with the increasing of the incident neutrino energy, the energy of recoil electron correspondingly increases, and the distribution exhibits more pronounced peak toward $\cos(\alpha) = 1$, indicating that the reconstruction with success is counted higher. As written in the panel, the efficiency η increases from 0.66% at $E_\nu = 2$ MeV to 66% at $E_\nu = 10$ MeV. The mean value of $\langle\cos(\alpha)\rangle$ as a function of the incident energy of the neutrino is displayed in panel (b). At the high energy end near 10 MeV, the mean value $\cos(\alpha) = 0.76$, suggesting a rather good determination of the direction of the electron. The distance ΔR between the genuine reaction vertex and the reconstructed one is presented in panel (c), as seen, the deviation of the reconstructed vertex decreases slightly as a function of the incident energy E_ν.

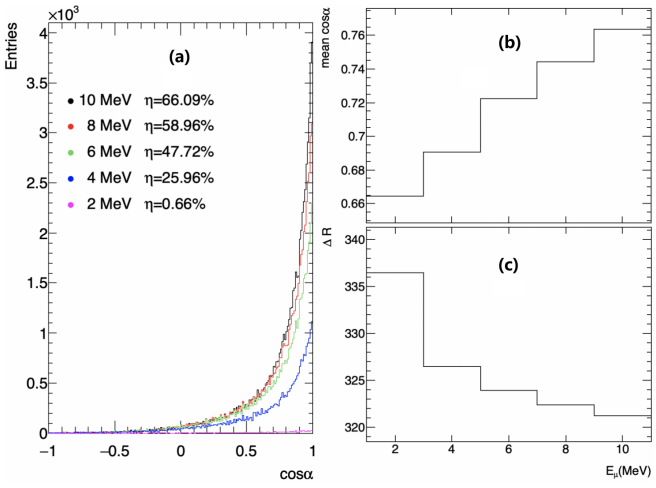

Fig. 9. (Color online) (a) distributions for angle construction with their efficiency. (b) and (c) show the mean value of $\langle\cos(\alpha)\rangle$ and the error of the constructed vertex as a function of the neutrino energy.

D. Influence of the background events

Careful treatments are required to suppress the events from the intense background, which includes the seawater radioactive isotopes and the cosmic-ray muons, as well as the faint light emitted by the bioluminescent planktons near the detector volume. In principle the muon background could be rejected at a high efficiency by a veto detector mounted above the detector or by the energy cut since the Čerenkov photons from the energetic muons penetrating the thick sea water are copious. Besides, the light from the bioluminescent planktons induces the signal on PMT with very different rising time and amplitude, and hence can be identified in principle. Here we mainly consider the sea water radioactivity, because the intensity of the γ radiation from the radioactive isotopes is high and the γ energy is comparable to the recoil electron in ν_e-e^- scattering, producing the main background noise, to which one shall be cautious and careful.

The primary and dominant radioactive isotope in seawater is ^{40}K. The mass fraction for potassium element in seawater is $\rho_{\rm k} = 380$ mg/L. The isotope abundance for ^{40}K is $\eta_{40} = 0.0117\%$. And the lifetime of ^{40}K is $\tau = 5.692 \times 10^{16}$s, so one calculates the event rate of ^{40}K from Eq. 6

$$n = \frac{\eta_{40} \cdot \rho_{\rm k} \cdot N_A}{M_{\rm k} \cdot \tau} = 12.03({\rm L}^{-1}{\rm s}^{-1}) \qquad (6)$$

where N_A is the Avogadro constant and $M_{\rm k}$ is the Molar mass of potassium element. The event rate is high as we expected, so it's necessary to have a simulation to this background. ^{40}K have several decay channels, γ delay give largest energy of 1.46 MeV to our detector, we assume a worst situation that all ^{40}K would decay from this channel which allow us to only simulate this intense radiation. To model the cascade interactions between γ with water, we directly inject 1.46 MeV γ with random direction and position as our background event. As γ could travel a distance before it is captured, we generate γ in an extended volume with the radius $R = 6$ m, which extends to larger range than the fiducial volume. Fig. 10 (a-c) presents the influence of the ^{40}K background. Panel (a) displays the distribution of $\cos(\alpha)$ with α being the angle of the reconstructed electron with respect to the 1.4 MeV γ rays from the source. The forward peaking feature is visible. Panel (b) shows the displacement of the real vertex and the reconstructed one. Panel (c) displays the distribution of the multiplicity of the fired PMTs $M_{\rm pmt}$ by the 1.4 MeV γ rays.

The other major radioactive source in seawater from the decay chain containing ^{232}Th and ^{238}U. The most energetic γ ray on the chain is the 2.6 MeV γ from ^{208}Tl. To be conservative, we simulate the background by using 2.6 MeV γ radiation. The same results are presented in Fig. 10 (d-f). It is shown that the feature of the 2.6 MeV γ is very close to that of 1.4 MeV γ ray, except that the multiplicity of fired PMT $M_{\rm pmt}$ is slightly higher. As seen at the peak positions, averagely the multiplicity of the 2.6 MeV γ background is higher than that of 1.4 MeV by 1 or 2 PMTs.

In order to discriminate the neutrino source from the background, one can impose a cut on $M_{\rm pmt}$ to suppress the events

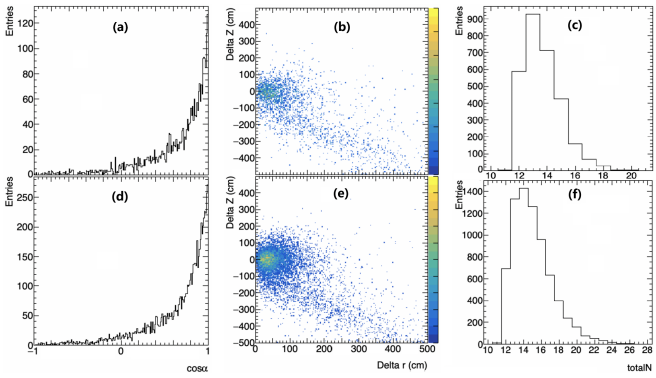

Fig. 10. (Color online) Left: The distribution of the angle between real and constructed direction of the γ rays at $E_\gamma = 1.4$ (a) and 2.6 MeV (d). Middle: the distribution of deviation between real and constructed vertex in coordinate space for the γ rays at $E_\gamma = 1.4$ (b) and 2.6 MeV (e) . Right: the distribution of the multiplicity of fired PMTs for the γ ray at $E_\gamma = 1.4$ (c) and 2.6 MeV (f).

induced by the intense radioactive source in the seawater. Figure 11 (a) presents the multiplicity distribution as a function of the incident neutrino kinetic energy E_ν. If a threshold condition $M_{\rm pmt} \geq 20$ is set on the multiplicity, as shown by the dashed line in panel (a), by increasing the neutrino energy, the events are increasingly accepted. The ratio of the events with the number of fired PMT above the threshold is 55% and 80% for $E_\nu = 6$ and 10 MeV, respectively, as shown in Fig. 11 (b). Filtering the HT procedure, the construction efficiency becomes 25.6% and 52.2%, respectively. This is still acceptable for detection. Whereas the events induced by the 1.4 MeV γ rays are suppressed by a factor of larger than 10^7.

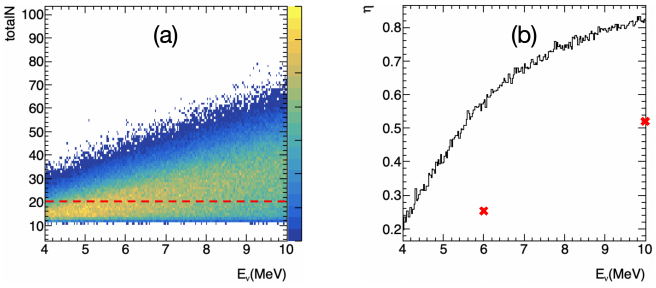

Fig. 11. (Color online) (a) Distribution of multiplicity of fired PMT number as a function of neutrino energy E_ν. (b) Ratio of the events above the $M_{\rm pmt}$ as a function of E_ν. The final reconstruction efficiency after HT transformation for 6 and 10 MeV neutrino is indicated by the red cross symbol.

IV. NEUTRINO SOURCE RECONSTRUCTION

With the background suppression scheme, now one can consider the simple application to identify an existed ν_e emission source, taking the sun as the example. The genuine ν_e induced events are drowned in the intense background. Since the radiation from ^{40}K is suppressed by 10^7, here the dominant background is not necessary ^{40}K. Instead, to make the scheme simple, the background events are added manually with arbitrary incident direction. In the meantime, the incident neutrino from the source position triggers a ν_e-e^- event, emitting the recoil electron which produces Čerenkov photons along the direction described by Fig. 8. To infer the location of the ν_e source, one shall accumulate certain number of ν_e-e^- scattering events and perform the Hough transform one more time.

Once the direction of the electron is reconstructed from the fired PMTs, one can perform the Hough transform using the probability distribution written in Eq. (4). Fig. 12 presents the transforming progress in θ-ϕ space. Totally 1000 events are used for searching. In panel (a) and (b), events are all neutrino signals, whereas in panel (c) and (d), ratio of background to signal is set to 5:1, where the background events (83%) are sampled randomly from all directions. The input source direction is set to meet an angle of 45° with respect to the axis in order to check the homogeneity of the detection ability, i.e., the initial directions are $\theta = 135^\circ$ and $\phi = 90^\circ$. In case of in panel (a), one can even distinguish by eyes that the dense population of events is visible in the vicinity of the set value. The Hough transform gives the most probable position in reconstruction situating at $\theta = 137.3^\circ$ and $\phi = 89.1^\circ$. However is panel (c), it's much harder to identify the source just from the data distribution plot. Still, Hough transform gives the constructed direction to be $\theta = 140.8^\circ$ and $\phi = 80.1^\circ$, which is only 8.8° deviation from the initial direction.

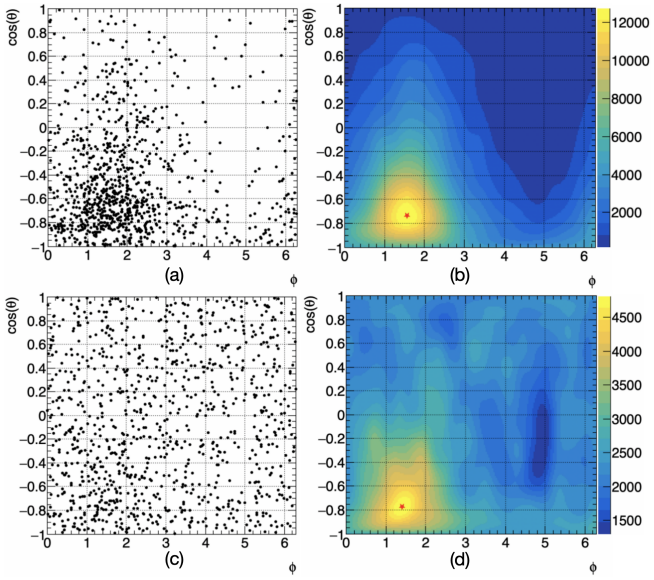

Fig. 12. (Color online) Plot of source searching Hough transform procedure. (a) data points of 1000 ν_e-e^- events. (b) The corresponding Hough transformed probability distribution in θ and ϕ space. (c) Data points of 1000 events with background-to-signal ratio being 5:1, where the background (83%) are from all directions randomly. (d) The corresponding Hough transformed probability distribution in θ and ϕ space.

Next, we estimate the solar neutrino flux and the event rate in the designed detector. We neglect the problem that the sun

is moving, because it can be cured by fixing the Z axis of our coordinate system to the sun and the expected incident direction is then fixed in the simulation. For solar neutrino with energy $E_\nu \geq 6$ MeV, the flux is approximately equal to $\Phi = 2.5 \times 10^6 \mathrm{cm}^{-2}\mathrm{s}^{-1}$ [32]. The energy dependent cross section of ν_e-e^-elastic scattering reads

$$\sigma = 93(E_\nu/\mathrm{MeV})(10^{-46}\mathrm{cm}^2) \quad (7)$$

The event rate can be calculated by

$$n = \rho\sigma\Phi = 0.005(\mathrm{m}^{-3}\mathrm{day}^{-1}) = 2(\mathrm{module}^{-1}\mathrm{day}^{-1}) \quad (8)$$

where $\rho = 0.56 \times 10^6 N_\mathrm{A}$ is the electron density in the water.

Considered the construct efficiency, we would expect the detected neutrino events to be about 20/module/month. Assuming there are 15 detect modules installed, one can get 300 solar neutrino events from same direction for each month. For background, since most of the events from ^{40}K are excluded by the cut condition, a background-to-signal ratio of 50 is a reasonable assumption, i.e., there are 15000 background events above the threshold. The background radiation is randomly sampled in all possible directions. With the signals and backgrounds as the input to the HT, the source direction can be inferred. Trying 10000 searches in simulation, the angle Θ_s between the real source direction and the reconstructed one is showing in Fig. 13. Defining the success reconstruction by $\cos\Theta_\mathrm{s} \geq 0.8$, as indicated by the dashed line, the success rate is about 90% for 30 days' search expecting 300 solar neutrino events.

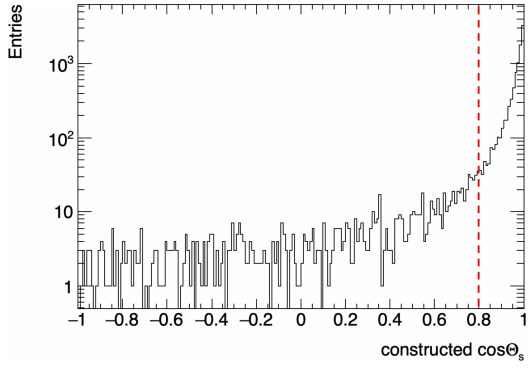

Fig. 13. Distribution of cosine of the angle ($\cos\Theta_\mathrm{s}$) between real and constructed neutrino source direction with 10000 simulated searches.

Finally, we investigate how the success search can be achieved as a function of the background-to-signal ratio achieved. It is important to design the experimental scheme, including the scale and the duration, since the number of signals in each search is proportional to the number of modules, or the total volume of the sensitive medium for detection, as well as to the length of searching time. Qualitatively, the more the neutrino signals, the more the search can be succeeded at larger background-to-signal ratio. One can simulate the background-to-signal ratio the search can be fulfilled at 90% success rate. The result is shown is Fig. 14. The minimum accumulation of events $N_\nu^{\min}(90\%)$ required to ensure 90% success rate is approximately linear to the background-to-signal ratio. It is seen that if the background-to-signal ratio is up to 270, it is necessary to accumulate 1000 neutrino events. From this relationship, one can estimate the mega volume of the detector modules at known neutrino flux and the background radiation intensity in deep sea water.

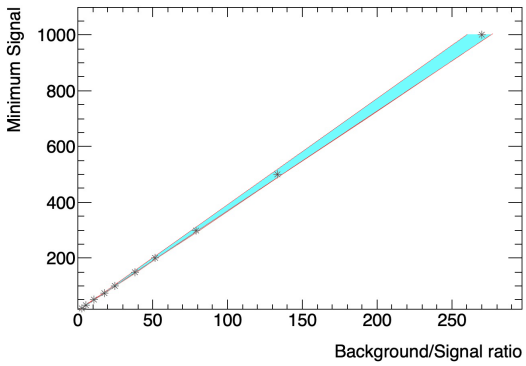

Fig. 14. (Color online) The minimum accumulation of events $N_\nu^{\min}(90\%)$ required to ensure 90% success rate as a function of background-to-signal ratio. The band represents a 99% confidence interval.

V. CONCLUSION

The proposal and feasibility to locate the neutrino source using deep sea water Čerenkov detector is discussed based on GEANT4 simulations. A spherical volume of water covered with PMT is constructed as the sensitive detector drown in sea water. The production and transport of Čerenkov photons generated by the ν_e-e^- reaction are simulated. The vertex and the direction of the high-speed electron producing the Čerenkov photons are reconstructed by using Hough transform. In order to detect the neutrinos, the background of γ radiation in sea water are taken into account with care. It is found that the background can be suppressed by setting a threshold on the number of firing PMTs. The reconstruction efficiency of the neutrino is 25% for 6 MeV neutrino and 52% for 10 MeV neutrino, respectively, showing an increasing trend with the neutrino energy. To locate an existing neutrino source, finite number of neutrino events are necessary, depending on the background intensity with the firing PMTs above the threshold. With 300 neutrino events accumulated, the source direction can be inferred with the angular accuracy $\cos\Theta_\mathrm{s} > 0.8$ under background-to-signal ratio of 50. The total volume and cost of the detector with sufficient counting rate may or may not limit the real application.

[1] Y. Fukuda et al., Phys. Rev. Lett. 81, 1158 (1998).
[2] Q. R. Ahmad et al., Phys. Rev. Lett. 89, 011301 (2002).
[3] H. Furuta et al, Nucl. Inst. Meth. A 662, 90 (2012).
[4] J. Ashenfelter et al., Nucl. Inst. Meth. A922, 287 (2019).
[5] G. Consolati et al, Nucl. Inst. Meth. A795,364 (2015).
[6] M. Battaglieri et al., Nucl. Inst. Meth. A 617, 209 (2010).
[7] N. S. Bowden et al., Nucl. Inst. Meth. A 572, 985 (2007).
[8] T. Classen et al., Nucl. Inst. Meth. A 771, 139 (2015).
[9] M. Kandemir and A. Cakir, Nucl. Inst. Meth. A 953, 163251 (2020).
[10] F. P. An et al., Phys. Rev. Lett. 108, 171803 (2012)
[11] J. Cao, Nucl. Inst. Meth. 732, 9 (2013).
[12] F. Reines, C. L. Cowan Jr., Nature 178, 446 (1956).
[13] F.P. An et al, Nucl. Inst. Meth. 811, 133 (2016).
[14] M. Abbes et al., Nucl. Inst. Meth. A 374, 164 (1996).
[15] A. Cabrera., Nucl. Inst. Meth. A 617, 473 (2010).
[16] K. Clark et al., Nuclear Physics B - Proceedings Supplements 233, 123 (2012).
[17] Z. P. Ye et al., Nature Astronomy volume 7, 1497–1505 (2023)
[18] M. Ageron et al., Nucl. Inst. Meth. A 656, 11 (2011).
[19] Y. Sestayo, Nucl. Inst. Meth. A 626-627, S196 (2011).
[20] A. Avrorin et al., Nucl. Inst. Meth. A 626-627, S13 (2011).
[21] U. F. Katz Nucl. Inst. Meth. A 626-627, S57 (2011).
[22] J. Brunner, Nucl. Inst. Meth. A 626-627, S19 (2011).
[23] R. Lahmann, Nucl. Inst. Meth. A 725, 32 (2013).
[24] D. Hellfeld et al., Nucl. Instr. Meth. A 841, 130 (2017).
[25] Z. Li et al., Nuclear and Particle Physics Proceedings 287, 147 (2017).
[26] The Water Cherenkov Simulator (WCSim). Repository: <https://github.com/WCSim>.
[27] R.S.J. Purser, Quarterly Journal of the Royal Meteorological Society 132, 619 (2006).
[28] K. Abe et al., Nucl. Instr. Meth. A 737, 253 (2014).
[29] M. Shiozawa, Nucl. Instr. Meth. A 433, 240 (1999).
[30] E.R. Davies, Machine Vision: Theory, Algorithms, Practicalities, Academic Press, San Diego, 1997.
[31] C. Giunti, C.W. Kim, Fundamentals of Neutrino Physics and Astrophysics, University Press, Oxford (2007)
[32] X.J. Xu et al., Progress in Particle and Nuclear Physics 131, 104043, (2023).